Senescent cell-derived extracellular vesicles recruit antigen presenting cells and limit squamous carcinoma recurrence

Ziglari T.[1], Claudio N.M.[1,3], Nakayasu E.S.[4], Kyle J.E.[4], Guo Z.[1,2], Pucci F[1,2,3]

[1]Department of Cell, Developmental & Cancer Biology, Oregon Health and Science University, Portland, Oregon

[2]Progman in Biomedical Sciences, Oregon Health and Science University, Portland, Oregon

[3]Department of Otolaryngology-Head and Neck Surgery, Oregon Health and Science University, Portland, Oregon

[4]Pacific Northwest National Laboratory, Richland, WA

Correspondence: pucci@ohsu.edu

Abstract

Senescent cell removal is a promising therapeutic approach to prevent and treat cancer. However, adverse reactions to current senolytic drugs, particularly, in geriatric populations with a compromised immune system and chronic inflammation, highlights a demand for research to develop targeted Immunotherapeutic. Cellular senescence is a cell autonomous tumor suppressor response to stressors that arrests cell cycle and initiates immune-mediated removal of senescent cells. Pathologic processes interfere with immune response leading to persistence of senescent cells and tumor progression. Investigating the communication pathways between senescent and immune cells has the promise of bringing to light therapeutic targets. Recently, it has been shown that senescent cells produce extracellular vesicles (EVs) containing signaling components resemblance to their parental cells. In order to study if and how senescent cell-derived extracellular vesicles (senEVs) contribute to immune-mediated removal of senescent cells, we inhibited EVs using dominant-negative mutant Rab35, while preserving soluble phenotypes. We then challenged C57BL6 mice with EV-inhibited or EV-competent senescent cells and evaluated immune infiltrates. Interfering with EV release led to the reduction of antigen-presenting cells including dendritic cells, macrophages, and B cells, which may contribute to the observed persistence of senescent cells. Interestingly, EV-inhibition reverted cellular senescence, promoted proliferation and tumor formation. Proteomic analysis revealed several proteins that were exclusively present on senEVs, compared to those from their non- senescent counterparts and some common biomarkers were found in two different cell lines. These results suggest that senEVs have a critical role in immune-mediated removal of senescent cells possibly via signaling to immune cells. Further investigations are required to declare common biomarker(s) on senEVs, which specifically are detected by immune cells.

Introduction

Head and neck squamous cell carcinomas (HNSCCs) originate from the squamous epithelium of the oral cavity, pharynx, and larynx and are the most malignancies that arise in the head and neck [1]. HNSCC is the 6th most common malignancy worldwide accounting for about 890,000 new cases and 450,000 deaths in 2018 [2, 3]. Almost 65,000 people are estimated to have been affected by HNSCC in the United States in 2019 [4]. The incidence of HNSCC continues to rise and is anticipated to increase by 30%, that is 1.08 million new cases annually, by 2030 [5]. Despite technological advances in cancer therapy including radiotherapy techniques, the development of bio-radiotherapy, and combinations of surgery and chemo-radiotherapy, only about 50% of patients respond to the front-line treatment [6]. The presence of advanced disease in the vast majority of patients is a major cause of recurrence and decreased survival with more than 50% of patients with regional or distant disease recurring within 3 years [7-9]. Only 10% of patients are progression-free 6 months after platinum-based chemotherapy, with immunotherapy merely doubling that figure [10], indicating that no therapeutic options prolong survival among these patients.

Current chemoradiation regimens exert their anti-tumor activity by switching cancer cells to a stable non-proliferative, metabolically active survival state named cellular senescence [11-13], which provides an immediate restriction in cancer cell propagation and tumor growth. However, compelling new data show that pathologic accumulation of senescent cells is implicated in a range of morbidities such as cancer recurrence [14, 15], both in a cell-autonomous and noncell-autonomous manner, respectively by escaping senescence and transitioning toward cancer stem-like state [16-19]. Furthermore, one of the hallmarks of senescent cells is producing a combination of soluble and insoluble components known as senescence-associated secretory phenotypes, SASP [18]. Although SASP suppresses tumor formation by blocking cell division and promoting immune clearance of damaged cells [20], it also drives tumor progression and cancer relapse [11, 21] via recruiting tumor-promoting immune cells followed by induction of chronic inflammation [20, 22, 23]. A growing body of evidence indicates that many malignancies arise from inflammation. The strong association of chronic inflammation with malignant diseases is shown in colon carcinogenesis, liver carcinoma, and stomach cancer arising in individuals with chronic ulcerative colitis, hepatitis, and chronic helicobacter pylori infection, respectively [24-26].

Overall, studies have reported that senescent cells have deleterious activities and have to be inhibited during cancer progression [27]. For example, co-injecting senescent human fibroblasts with epithelial cancer cells stimulates hyper-proliferation of preneoplastic, but not normal epithelial cells and accelerates tumor growth *in vivo*. These results may seem at odds with the tumor suppression function of cellular senescence [28]. These studies indicate that removal of senescent cells after induction of senescence is critical to improve survival of patients with advanced HNSCC and other solid cancers. It is therefore important to develop strategies to eliminate senescent cells. Our preliminary evidence suggested that senescent cell removal depends, at least in part, on senescent cell-derived extracellular vesicles (senEVs). SenEVs are nanometer-sized membrane-bound particles containing various signaling molecules that are emerging as novel class of SASP [29-31]. Due to simplicity of their isolation, the resemblance to their parental cells, and the less variability of their signaling clusters compared to those in their parental cells, circulating senEVs have raised considerable interest as a source for the induction of homogeneous immune response. These unique characteristics plus their abundances in all body fluids such as blood, saliva, and urine highlights senEVs as useful targets for liquid biopsy, which is simpler and less invasive than conventional diagnostic methods [29-33]. However, little is known about the role of senEVs in senescence surveillance. The goal of the current study was to address this issue by profiling immune cells, which infiltrate sites of senescence in presence and absence of senEVs. Our data support a scenario in which chemotherapy-induced senescence promotes the release of senEVs carrying a set of distinguishing antigens. senEVs contribute to immune-mediated clearance of senescent cells by recruiting antigen presenting cells, and in their absence, senescent cells persist in tissues, increasing the risk of tumor formation. However, as senescent cells are highly heterogeneous in both their molecular biology and their physiological function, identification of universal markers provides promising therapeutic approaches to prevent and treat cancer. In order to find out the common biomarkers on senEVs, we will further identify candidate therapeutic targets on immune cells and will determine the role of adaptive immune responses toward senEV antigens in senescence surveillance.

Materials and Methods

Cell culture media and reagents

The cell lines used in this study were Oral Epithelial Squamous Cell Carcinoma (MOC2 and mEER+). MOC2 carries the same mutations observed in human head and neck cancers, namely Trp53, MAPK and FAT [34] whereas mEER+ have been engineered to express Hras(G12) and HPV-E6/E7 [35]. Paclitaxel from Taxus brevifolia >95% and Cisplatin Pharmaceutical Secondary, Dulbecco's Modified Eagle's, Dispase II, BCA protein

assay kit, Insulin, were purchased from Sigma-Aldrich. Cellular Senescence detection kit was purchased from Dojindo. Amicon ultra-15 centrifugal filters UFC910024, 100 kDa, Licor IRDye 800CW Streptavidin, Trypsin EDTA were purchased from Fisher Scientific. Phase-flow Alexa fluor 647 BrdU kit, BrdU, Anti-BrdU antibody, Annexin V Binding buffer, FITC annexin V were purchased from Biolegend.

Cell lysis buffer was purchased from Cell Signaling Technology. Anti-rabbit detection module for Wes, 12-230 kDa Wes Separation module were purchased from ProteinSimple. Proteome Profiler mouse cytokine array was purchased from R&D systems.

Culture medium tested in this study was E-media prepared by adding 1:1 ratio of Iscove's Modified Dulbecco's Medium (IMDM) with HEPES without L-Glutamine (purchased from Lonza), and Dulbecco's Modified Eagle Medium (EMDM)/F12 1:1 with 1.0 g/L glucose, with HEPES (25 mM), without L-Glutamine (purchased from Fisher Scientific). The above-mentioned combined medium was supplemented by adding 10% Fetal bovine serum (FBS, from VWR), 0.5% Penicillin/Streptomycin Solution (from GE Healthcare), 25µg/µl Hydrocortisone (from Sigma), 0.25 µg/µl Cholera toxin (from Sigma), 25 µg/µl Transferrin (from Sigma), 10 µg/µl Insulin (from Sigma), 0.2 µg/µl Tri-Iodo-Thyronine (from Sigma), and 10 µg/ml E.G.F (from Gibco). MACS buffer was prepared by adding 2 mM EDTA (From Fisher Scientific), 0.5% BSA (from Fisher Scientific) to 500 mL PBS.

Mice, engraftment models and evaluation of immune responses

Eight- to 12-week-old male and female C57BL/6 mice were bred in animal facility of OHSU. The mice were maintained under conventional conditions. For tissue engraftments, mice were anesthetized with inhalant isoflurane and confirmed the success of anesthesia by the lack of reaction to toe pinch. For tumors intentionally implanted Intradermally, a total of 0.5*10^6 or 1*10^6 cells (depending on the purpose of study) suspended in 50 µl filtered PBS were injected into flank. For this purpose, the beveled tip of the needle was inserted face up at a <10-degree angle and advanced 2-3 mm into the tissue parallel to the skin while lifting the needle to create a tenting effect. This resulted in a well-demarcated weal and could be felt as pressure or resistance during injection. For orthotopic xenografts, a total of 0.5*10^6 cells in a total volume of 20 µl were injected into the central portion of the tongue.

In order to determine tumor volume by external caliper, the greater longitudinal diameter (length) and the greatest transverse diameter (width) were determined twice a week after injection. Tumor volume based on caliper measurement were calculated by the modified ellipsoidal formula as follows:

Tumor volume= 1/2 (length * width^2)

To evaluate the immune response against the tissue engraftment, following CO2 asphyxiation, the site of injection (either with a growing mass or without) as well as draining and non-draining lymph nodes were dissected and washed briefly in 1XPBS and weighed. Depending on the requirement of the experiment, they were either fixed for 10 min with 4% PFA or dissociated as follows: tissues were minced with scissors and homogenized in dissociation media and incubated at 37C, 500rpm for 30 min in heater-shaker. After dissociation, the tissues were washed on 100 µm strainer with 50 ml of MACS buffer and centrifuged at 500g for 10 min. The pellets were pipetted in the corresponding wells of a deep 96-well plate on ice and mixed with a mixture of corresponding surface antibodies plus beads. Extra pellets were stained with corresponding antibodies for fluorescence minus one (FMO) control. The plates were sealed with adhesive film and incubated on ice for 30 min at the dark. After incubation, the cells were washed twice with PBS and centrifuged at 500g for 5 min, then, they were stained with zombie dye and incubated for 15 min on ice at the dark. The cells were then washed with PBS and gently vortexed to dissociate the pellets and fixed and permeabilized with True-nuclear transcription factor buffer set according to the manufacturer's guidelines. Briefly, cells were fixed with 1X fix concentrate and incubated at room temperature for 30 min and permeabilized by adding 1X perm buffer. Cells were washed three times in 1X perm buffer and vortex gently after resuspension in perm buffer. Then a mixture of corresponding intracellular

antibodies in 1X perm buffer were added to the cells and incubated overnight at 4C in the dark. The antibodies were removed by washing with perm buffer and resuspending in MACS buffer. The readout was done with Fortessa flow cytometer.

Flow cytometry analysis of immune cells was according to the following gating:

First *in vivo* experiment:

Neutrophils: Zombie -, CD45+, Ly6G+, F4/80-

Tissue macrophages: Zombie -, CD45+, Ly6G-, F4/80+, CD80-, MHCII+

Recruited macrophages: Zombie -, CD45+, Ly6G-, F4/80+, CD80+, MHCII-

Macrophages: Zombie -, CD45+, Ly6G-, F4/80+, CD80-, MHCII-

B cells: Zombie -, CD45+, Ly6G-, F4/80-, B220+, CD3-

Dendritic cells: Zombie -, CD45+, Ly6G-, F4/80-, B220-, CD3-, MHCII+, NK1.1-

NK cells: Zombie -, CD45+, Ly6G-, F4/80-, B220-, CD3-, MHCII-, NK1.1+

NKT cells: Zombie -, CD45+, Ly6G-, F4/80-, B220-, CD3+, NK1.1+, CD4-

T cells: Zombie -, CD45+, Ly6G-, F4/80-, B220-, CD3+,

T regulatory cells: Zombie -, CD45+, Ly6G-, F4/80-, B220-, CD3+, FoxP3+

T helper cells: Zombie -, CD45+, Ly6G-, F4/80-, B220-, CD3+, CD4+, Tbet+

Second in vivo experiment:

Dendritic cells: Zombie -, CD45+, B220-, F4/80-, 103+, XCR1+, MHCII+

B cells: Zombie -, CD45+, B220+, F4/80-, MHCII+, CD3-, NK1.1-, Ly6G-,

Functional B cells: Zombie -, CD45+, B220+, F4/80-, MHCII+, CD3-, NK1.1-, Ly6G-, CD80+, CD86+

Macrophages: Zombie -, CD45+, B220-, F4/80+MHCII+, CD206-,

Induction of Senescence *in vitro* using chemotherapeutic agents or irradiation

In order to optimize the induction of senescence in MOC2 or mEER+ using chemotherapeutic agent(s), a matrix of Paclitaxel (0-1000 nM) and/or Cisplatin (0 µM-48 µM) were used. MOC2 and mEER+ were expanded in E-media and plated at 20,000 cells/well in 96-well plate at 37C and under 5% CO2 for 24 hrs. The above-mentioned ranges of Paclitaxel and/or Cisplatin were added to the cells and incubated for additional 48hrs at 37C in 5% CO2. The irradiation assay was performed with a dose rate of 2.5 or 5 Gray. All irradiation experiments were performed on 1-day old cells cultured in 6-well plates in E-media.

Flow cytometric detection of SA-B-Gal

One of the most widely used markers of senescence is the increased levels of senescence-associated B-galactosidase (SA-B-gal) activity [36]. The cell permeable, intracellular retentive substrate, SPiDER-B-Gal, immediately forms a quinone methide that acts as electrophile when proteins containing nucleophilic functional groups are nearby the molecules. By the probe undergoes the reaction with a protein, the conjugates become fluorescent compounds with high sensitivity, which can be applied to quantitative analysis by flow cytometry. Because most cells express endogenous B-galactosidase enzymatically active at pH 4.0, SA-B-Gal is assayed by staining at non optimal pH 6.0 using Bafilomycin A1 to better differentiate normal and senescence cells. The analysis of cellular senescence was performed using the cellular senescence detection kit SPiDER-B-Gal. All steps were performed according to the manufacturer's instructions. Briefly, after treatment with Paclitaxel and/or Cisplatin for 48 hrs as described above, the cells were washed with PBS and cultured in an incubator at 37C with 5%CO2 for 1 hr after adding Bafilomycin A1 solution. Then, the cells were incubated for an additional 30

min after adding SPiDER-B-Gal solution. The cells were washed with PBS and digested with EDTA-free trypsin. The cells were collected in round-bottom 96-well plate containing MACS buffer after centrifugation 800 rpm for 5 min. Finally, a flow cytometer (BD Biosciences) was used for detection in high throughput mode. The excitation and emission wavelengths for SA-B-Gal are 488 and 530 nm, respectively.

The parallel plates were prepared to test the unwanted induction of apoptosis and/or cell death by Paclitaxel and/or Cisplatin. For this purpose, after discarding the E-media containing Paclitaxel and/or Cisplatin, the cells were washed with PBS and harvested by trypsin and resuspended in 50 µl FITC Annexin V working solution (3% FITC Annexin V and 3% 7-AAD in Annexin B binding buffer) and incubated for 15 min at room temperature at dark. FITC Annexin V working solution was discarded and cells were resuspended in MACS buffer and cells were observed by flow cytometer (488nm/525nm and 550nm/650nm).

BrdU procedure

Thymidine analog 5-bromo-2-deoxyuridine (BrdU) has been widely used in the last decades as gold standard of assessing cell proliferation by quantifying the percentage of DNA-synthesizing cells [37]. The BrdU labeling was performed according to the manufacturer's guidelines. Briefly, MOC2 and mEER+ squamous cell carcinoma lines were plated at 20,000 cells per well in a 96-well plate and allowed to be 70% confluent for 24 hrs at 37°C, 5% CO2. The day after, the cells were exposed to the chemotherapeutic agents and incubated for 48 hrs. After washing the cells with media, the cells were pulsed with 5 µg BrdU per well for 2, 4, or 24 hrs (depending on the goal of study). Cells were washed, fixed, and permeabilized with the corresponding buffers and then treated with DNase for 1 hr. Cells were washed and stained with 1µg anti-BrdU antibody per well for 30 minutes, then washed and the signals acquired on a flow cytometer.

Western blotting for qualification of EVs

Ultrafiltration EV-depleted FBS was prepared as described elsewhere [38]. Briefly, regular FBS was centrifuged in Amicon ultra-15 centrifugal filters for 55 min at 3,000 g. The flow-through was collected and added to the E-media (10%). WT MOC2, which was competent for EV production and Rab35 DN MOC2, which was suppressed for EV production were cultured in E-media containing EV-depleted FBS for 72 hrs. Supernatants were collected and normalized based on the number of the cells, then, centrifuged at 2000 rpm for 10 min. Supernatant was transferred to UC tubes and centrifuged for 24200 rpm at 20C for 70 min. The supernatants were discarded and the tubes were kept upside down on tissue papers for 1 min, then, 50 µl of 0.2µm filtered PBS was added to each tube, after pipetting several times, the EVs were collected and stored at -20C upon use. Western blot was performed to detect EV marker, Flotillin-1 by rabbit anti-Flotillin-1 using Simple western system according to the manufacturer's guideline. Briefly, 1XCST buffer containing proteinase inhibitor was added to the EVs and vortexes several times. One part of 5X Fluorescent Master Mix was added to the four parts of the lysed EVs and denatured at 95C for 5 min along with ladder and then were transferred on ice. The final concentration of Flotillin-1 and Rabbit anti-Flotillin-1 were optimized as 0.4 mg/ml and 1:50, respectively.

Nanoparticle tracking analysis for quantification of EVs

The quantification of EVs was performed using Zetaview based on two independent methods, light scattering/particles' Brownian motions and a membrane intercalating dye, Di 8 ANNEPS. WT MOC2, which was competent for EV production and Rab35 DN MOC2, which was suppressed for EV production were cultured in E-media containing EV-depleted FBS for 72 hrs. Supernatants were collected and normalized based on the number of the cells, then, centrifuged at 1000 rpm for 10 min. Supernatant was collected and kept at -20C upon use. EV-free media was diluted 1:1000 in filtered PBS and was used to set the sensitivity of the Zetaview. Supernatants were diluted 1:1000 in filtered PBS and the size and the number of the particles was measured.

Alternatively, Di 8 ANNEPS working solution was made by adding 1% Di 8 ANNEPS and 0.25% Pluronic F-127 in PBS. The supernatants containing EVs were incubated with Di 8 ANNEPS working solution in 10:1 ratio for 10 min at room temperature. Then, they were diluted by adding 1 ml PBS and were applied in Zetaview by selecting the laser 488 nm and the filter 500 nm.

Cytokine/Chemokine expression in cells

Expression levels of cytokines and chemokines in cell supernatants were quantified using Proteome Profiler Mouse Array Kit. For this purpose, supernatants of cells were collected after incubation of cells for 48 hrs. Array membranes were incubated and developed with the supernatants mixed with biotinylated specific detection antibodies following the manufacturer's instructions. However, for the detection of cytokine/chemokines, HRP-conjugated Streptavidin was replaced by IRDye 800CW Streptavidin and arrays were scanned simultaneously using a Li-Cor Odyssey imaging system, which provides a near-infrared fluorescence (NIR) detection. The advantage of NIR detection is that protein expression can be measured over a much wider linear dynamic range compared to that allowed by chemiluminescence methods. This approach facilitates accurate analysis of weak and strong spots on the same membrane without the uncertainty and inconvenience of multiple exposures. In addition, NIR doesn't require film and chemicals for development or the use of dark room. The mean pixel intensity for each signal was analyzed using ImageJ.

Mass spectrometry

Proteins were extracted using a modified Folch extraction [39]. Briefly, samples were extracted with chloroform/methanol (2:1, v/v) in a 4-fold excess to the sample volume to yield a hydrophobic layer containing lipids and a protein disc. Each layer was transferred to separate glass autosampler vials and the protein pellet was washed with 1 mL of ice-cold methanol. Each sample was evaporated to dryness in vacuo, and appropriately stored at -20˚C until further processing and analysis.

Proteins were dissolved in 8M urea prepared in 50 mM NH_4HCO_3, pH 8.0, containing 5 mM dithiothreitol and reduced for 30 min at 37 ºC. Cysteine residues were alkylated for 30 min 37 ºC with a final concentration of 10 mM iodoacetamide from a 500 mM stock solution. Samples were diluted 8-fold with 50 mM NH_4HCO_3, pH 8.0 and 1 M $CaCl_2$ was added to a final concentration of 1 mM. Proteins were digested with sequencing-grade modified trypsin (Promega, Madison, WI) overnight at 37 ºC. Samples were submitted to solid-phase extraction using C18 spin columns (Ultramicrospin columns, C18, 3- to 30-µg capacity; Nest Group), as previously described [40].

Peptides were separated on a capillary column (60 cm x 50 µm ID packed with C18, 3-µm particles) using a gradient of acetonitrile (mobile phase B) in water (mobile phase A), both supplemented with 0.1% formic acid. The elution was carried with the following gradient: 2 min, 8% B; 20 min, 12% B; 75 min, 30% B; 97 min, 45% B; 100 min, 95% B; 105 min, 95% B; 115 min, 1% B; 120 min, 1% B. Eluting samples were analyzed on a Q-Exactive mass spectrometer (Thermo Fisher Scientific). Full scan spectra were collected in a range of 300 to 1800 m/z with a resolution of 70,000 at m/z 400. The 12 most intense parent ions with multiple charges were submitted to high-energy collision dissociation with 33% normalized collision energy at a resolution of 17,500. Each parent ion was fragmented once and then excluded for 30 sec.

LC-MS/MS data was processed with MaxQuant [41] by searching tandem mass spectra against the human sequences from Uniprot Knowledge Base. Intensity-based absolute quantification (iBAQ) method was used for quantification [42].

Statistics

Statistical analysis of the results was performed using One-Way ANOVA analysis of variance with a confidence interval of 95% and corrected for multiple comparisons using the Holm Sidak algorithm in GraphPad Prism version 7.03. Proteomic results were analyzed using R. P values < 0.05 were defined as significant.

Results

Development of an engraftment-based senescence model

Squamous cell carcinoma is the most frequent histological subtype of head and neck tumors, making up to 95% of the cases. Cellular senescence is commonly found in precursor lesions leading to HNSCC in patients [43]. These pre-malignant lesions do not contain carcinoma cells, only senescent and immune cells. Furthermore, current chemoradiation regimens exert their anti-tumor activity by switching cancer cells to senescent cells [11], which provides an immediate restriction in cancer cell propagation and tumor growth. However, compelling new data show that senescent cells can drive cancer recurrence [14, 15] by escaping senescence and transitioning toward a cancer stem-like state [16-19] or by recruiting tumor-promoting immune cells via release of pro-inflammatory mediators [25, 26] collectively known as SASP [20]. The paradoxical influence of cellular senescence on cancer relapse is a knowledge gap that must be urgently filled to improve survival of patients with advanced oropharyngeal SCC and other solid cancers. Unfortunately, systemic treatment with senescence-inducing stimuli, such as chemotherapeutics or irradiation, inevitably also affects hemopoiesis and immune responses, which represent a major obstacle in the study of senescence surveillance. To model precursor lesions without altering endogenous immune cells, we set to develop and characterize an engraftment-based senescence model. To this end, we validated *in vitro* methods to induce senescence in oral epithelial squamous cell carcinoma lines (named MOC2 and mEER+). MOC2 carries the same mutations observed in human head and neck cancers, namely Trp53, MAPK, and FAT [34], whereas mEER+ have been engineered to express Hras(G12) and HPV-E6/E7 [35]. Together the mutational landscape of these two cell lines model >95% of human pathology [44].

As senescence-inducing stimuli, we employed two chemotherapeutic agents, paclitaxel and cisplatin, as well as X-ray irradiation, which are commonly used as first-line methods in HN cancer patients [45, 46]. In order to optimize the dose, we employed a range of paclitaxel (0-750 nM) and/or cisplatin (0-35 µM) for the above-mentioned cells for 48 hrs and then quantified senescence by measuring senescence-associated Beta-Galactosidase (SA-B-Gal) activity, which is a widely accepted marker of senescence [47]. A defining feature of cellular senescence is the permanent exit from cell cycle, while maintaining cell viability. To confirm that paclitaxel treatment generates *bona fide* senescent cells, we assessed proliferation, apoptosis and cell death, or lack thereof. We measured proliferation of the cells using BrdU assay [37], apoptosis using Annexin V and cell death using 7-AAD. In the cells treated with paclitaxel and/or cisplatin, we identified the optimal dose able to induce senescence and inhibit proliferation in virtually all the cells without induction of significant apoptosis or cell death (Figure 1A & Figure S1). The results of SA-B-Gal was consistent with the morphological changes of the cells after exposure to chemotherapeutic drugs (Figure S1) as senescent cells exhibit an enlarged and flattened morphology [48]. Although maximum senescence was induced when treating MOC2 or mEER+ with 600 nM paclitaxel and 4µM cisplatin, the addition of cisplatin had a negative impact on the cell number and viability of

recovered cells for implantation in mice (Figure 1A and S1), therefore, cisplatin was excluded from the senescence-inducing treatment in subsequent experiments. Paclitaxel alone was enough to virtually block proliferation of these fast-growing squamous cell carcinoma lines by reducing maximum proliferation to 15% and slowing proliferation rate 7-fold, for a combined 98% reduction in proliferation potential (Figure 1B). To identify optimal dose of X-ray irradiation, we employed one, two, or three doses of 2 or 5 gray and incubated the cells for one, two, or three days after the last exposure. Although in most experimental conditions, X-ray could induce senescence, it could not efficiently inhibit cellular proliferation (Figure S2), which remained a main drawback for x-ray optimization. It is possible that the cells exposed to X-ray have expressed senescence markers prior to cell cycle arrest [49]. Higher dose of X-ray (10 Gray) resulted in significant cell death (data not shown). Therefore, irradiation was also excluded from the senescence-inducing treatment and the study was continued with paclitaxel 600 nM.

After engraftment in mice, *in vitro*-generated senescent cells are not exposed anymore to paclitaxel. To assess if engrafted senescent cells remain senescent in the absence of paclitaxel, we measured SA-B-Gal activity in paclitaxel-treated cells after removal of paclitaxel from cell culture media. We observed that the senescent phenotype remained present for at least a week (Figure 1C), suggesting that engraftment of senescent cells in animals may represent a viable option to generate a model of *in vivo* senescence. However, the environment found by senescent cells in the tissue is likely very different from the culture dish. To test if, once *in vivo*, senescent cells would revert to squamous carcinoma cells and form a tumor, we compared tumor formation in immunocompetent syngeneic mice between untreated squamous carcinoma cells and paclitaxel-treated squamous senescent cells. After implanting the same numbers of squamous carcinoma cells and senescent cells, we observed that paclitaxel treatment completely abated tumor formation, for at least 3 weeks (Figure 1D), indicating that paclitaxel treatment induces a *bona fide* senescence state in squamous carcinoma cells.

Removal of senescent cells is mediated by immune responses [50]. The immune response found during senescence surveillance is believed to be different from that elicited within the tumor microenvironment [51, 52]. To test whether our engraftment model of senescence recapitulates these differences, we studied immune responses in orthotopic settings by injecting either senescent squamous cells, squamous carcinoma cells or PBS in the tongue of mice. We performed multiparameter flow cytometric analysis of the tissues 3 days after engraftment. When we compared senescence and tumor models, we observed significant differences in their immune infiltrates (Figure 1E). As expected, T and NK cells were significantly increased within senescent tissues 3 days after challenge. We also observed a significant shift in macrophage subsets, with an increase in the fraction of MHC-II– CD80+ CD206+ macrophages and a corresponding decrease in the MHC-II+ CD80– CD206– macrophages (Figure 1E). Interestingly, B cells trended toward a decrease in senescent tissue. All of the above-mentioned immune subsets were differently recruited by tumor and senescent cells. On the contrary, neutrophils, regulatory (FoxP3+) and type-1 helper (Tbet+) T cells were coordinately recruited by both tumor and senescent cells (Figure 1E). These results suggest that our senescence model recapitulates expected immune responses and that there are shifts in immune cell infiltrates during senescence surveillance. These changes in immune composition may play important roles in the removal of senescent cells. Overall, these results confirm that we have successfully generated an *in vivo* model of senescence that does not rely on systemic administration of chemotherapeutic agents.

Inhibition of EV release in senescent cells does not alter senescence-associated secretory phenotype

Our previous work was among the first to study endogenously released extracellular vesicles (EVs) and their roles in communicating with immune cells in the context of cancer [53]. In this study, we repurposed some of our genetic tools to investigate the functional role of unmanipulated EVs in cellular senescence. To this end, we inhibited EV release from senescent cells *in vivo* and quantified changes in immune infiltrations. To interfere with senEV release, we used an approach we successfully employed in melanoma cells. We and others previously demonstrated that a dominant-negative mutant of Rab35 (Rab35 DN) greatly reduces the release of EVs, resulting in EV-deficient cells [53-55]. As control, we over-expressed wilt-type Rab35 (EV-competent cells). We carefully validated that over-expression of Rab35-DN efficiently and specifically reduces EV release also in senescent cells, while avoiding any unwanted impact on the SASP. To this end, we performed immunoblot assays for EV marker Flotillin-1 on the EV fraction of senescent and squamous cell carcinoma supernatants. After normalizing cell number, we observed almost complete absence of EVs in both senescent and non-senescent carcinoma cells expressing Rab35-DN (Figure 2A). These results indicate that the profound inhibition of senEV release is suitable for functional studies. We further validated EV inhibition using an independent technique, nanoparticle tracking, which measures EV numbers and size. Although nanoparticle tracking measurements suffer from high background levels, we confirmed a 4-to-6-fold decrease of EV release from senescent cells expressing Rab35-DN (Figure 2B). A caveat of interfering with vesicular trafficking via Rab35 is that certain SASP factors may be decreased as well. In order to test whether Rab35-DN over-expression in senescent cells inhibits SASP components, we quantified 40 different soluble factors from cell culture supernatants (Figure 2C). Of these 40 mediators, 8 were expressed at significant levels (G-CSF, GM-CSF, CXCL10, CXCL1, M-CSF, CCL2, CXCL2 and TIMP1), and are all well-established SASP factors [56, 57]. Two of these 8 SASP factors (CCL2 and CXCL2) were actually expressed at slightly higher levels in senescent cells after EV inhibition. An additional 6 mediators (IL1a, IL5, IL17, CCL5, CXCL12 and TNFa), were expressed at low but detectable levels and were unaffected by expression of Rab35-DN. Overall, these results indicate that over-expression of Rab35-DN is a valuable approach to significantly and specifically decrease EV release from senescent cells, without compromising the composition of the SASP.

Senescent-cell derived extracellular vesicles recruit antigen-presenting cells to the site of senescence

After setting up a *bona fide in vivo* model of senescence that recapitulates the expected immune composition of senescent tissues, and after comprehensive validation of EV inhibition in senescent cells, we turned to functionally investigate the role of senEVs in senescence surveillance by immune cells. Recruitment of immune cells for senescence surveillance is mediated by the SASP [21, 58-60]. EVs are emerging as important components of the SASP [29, 30, 32, 61]. We wanted to understand if senEVs have a functional role in senescence surveillance and tumor formation/recurrence. To test this *in vivo*, we challenged mice with half a million senEV-competent or senEV-deficient senescent cells. Our *in vitro* senescence induction protocol reduced total cell proliferation to 15% (as compared to untreated squamous carcinoma cells, Figure 1B), and slowed cell cycle down by a factor of 7 (after a 2-hour BrdU pulse, Figure 1B), which is equivalent to a 98% reduction in cell proliferation potential. Strikingly, senEV inhibition promoted tumor recurrence in two independent experiments, as compared to EV-competent senescent cells (Figure 3A). We validated if senEV inhibition interferes with paclitaxel-induced senescence. Of note, Rab35 manipulation did not influence senescence induction or exit from cell cycle (Figure 3B), suggesting no cell autonomous effects of senEV inhibition. To start investigating the fate of engrafted senescent cells in immune competent mice, we repeated the experiment and tracked the numbers of engrafted senescent cells using genetic markers 3 days after implantation (that is, when there is no visible tumor formation yet). We observed that senEV-competent senescent cells were quickly reduced to almost undetectable levels, whereas interfering with senEV release led to longer persistence of senescent cells, which was 5-fold higher than that of senEV-competent senescent cells, on average (Figure 3C). These results suggest

that senEVs may play non-cell-autonomous roles in senescence immune surveillance by promoting senescent cell removal from tissues, which ultimately prevents cancer recurrence.

To functionally investigate the role of senEVs in senescence immune surveillance, we repeated the experiment above and challenged mice with half million senEV-competent or senEV-deficient senescent cells. After 3 days (that is, when there is no tumor yet), we quantified the immune infiltrate, including CD4 and CD8 T cells and their type-1 effector subsets expressing T-bet, T regulatory cells, NK and NKT cells, myeloid cells including neutrophils, dendritic cells, macrophages and their subsets, and B cells. We observed a significant decrease (~50%) only in specific immune cell types, which were related only by the fact that they are all professional antigen presenting cells (APC); senEV inhibition decreased the fractions of infiltrating dendritic cells, B cells and MHC-II+ macrophages (Figure 3D). The decrease in immune infiltration can explain the persistence of senescent cells in tissues (Figure 3C), which can lead to tumorigenesis. Interestingly, senEVs increased the fraction of activated, MHC-II+ macrophages, indicating that senEVs may also have a role in activation of immune cells. These results strongly suggest that senEVs recruit and activate antigen presenting cells, which may find in senEVs a source of senescent cell antigens. Overall, these observations are consistent with a model in which senEVs promote immune surveillance of senescent cells. The recruitment of APC suggests that senEVs may represent a source of senescent cell antigens for adaptive responses. If senEV signaling is impaired, senescent cells will persist longer in tissues, which increases the chances of recurrence.

Proteomic profile of senescent cell-derived EVs (senEVs)

Senescent cells possess a different gene expression profile than normal cells [62, 63]. To date no studies have investigated the protein composition of EVs from senescent squamous cells. To start filling this gap and to identify which signals on senEVs may be responsible for the observed recruiting and activating APC (Figure 3D), we compared EVs from senescent and tumor cells. We quantified protein content, numbers and size by mass-spectroscopy, electron microscopy and nanoparticle tracking analyses. Senescent cells released ~6-fold higher amounts of EVs per million cells, as measured by protein content, compared to non-senescent squamous carcinoma cells (Figure 4A). These results may be explained by either a higher rate of EV release by senescent cells, a bigger size, or higher amounts of proteins among their cargo, or a combination of the above. To discriminate between these alternatives, we performed nanoparticle tracking analysis (Figure 4B). After normalizing cell numbers, we observed that senEVs had a 2-fold lower count compared to EVs from non-senescent cells (not shown), which resulted in a ~13-fold higher protein content per single EV (Figure 4B, right). We observed a 16% increase in median diameter, as measured by nanoparticle tracking analysis (Figure 4B left), which corresponds to a 60% increase in volume (assuming a spherical shape). Electron microscopy analysis confirmed that senEVs are 16% bigger than tumor EVs (Figure 4C). These results indicate that senEVs are bigger and pack more proteins, as compared to tumor EVs. The increase in senEV protein content and size suggests that they may carry important signals for immune cell recruitment and/or activation. To identify senEV-specific proteins that may signal immune cells, we performed proteomic analyses. We scaled up senescent cell production *in vitro* (validation data not shown) and used mass spectroscopy to analyze EVs, in collaboration with the Pacific Northwest National Laboratories. We isolated EVs by ultracentrifugation from cell culture supernatants. In order to avoid contamination from fetal bovine serum EVs, we cultured the cells using EV-free serum. Proteomic analysis revealed 150 and 120 proteins differentially present in senEVs from MOC2 and mEER+ cells, respectively (as compared to EVs from non-senescent MOC2 and mEER+, Figure 4D). Proteins in senEVs were significantly associated with pathways involved in core cellular functions (Ribosomes, Spliceosome and DNA replication) but also with type-1 immunity (systemic lupus erythematosus; Figure 4E). Among the proteins found in common between mEER+ and MOC2 (which carry different mutations/oncogenes,

see above), ribosomal proteins were the most common (Figure 4F). Overall, these results indicate that senEVs carry a unique set of molecules that may signal to immune cells. Further investigation is required to clarify any correlation between these molecules on senEVs and the observed immune response against senescent cells.

Discussion

The persistence of cellular senescence is detrimental as it is commonly found in precursor lesions leading to HNSCC in patients [43] and it can drive cancer recurrence [14, 15] after chemoradiation regimens, which initially trigger cellular senescence [11] to stop growth of any residual tumor cells. Such senescence paradox is a knowledge gap that must be urgently filled to address the unmet medical need of cancer relapse. Historically, cellular senescence has been defined as the permanent exit from the cell cycle [64]. Recent investigations suggest that cellular senescence may not be as permanent as previously thought, and propose that senescent cells can escape senescence and become cancer stem cells, in both solid and liquid tumor types [16-19, 65]. Despite changes in the definition of senescence, the presence of SASP remains a hallmark of senescence. The SASP is composed of several different families of soluble mediators and EVs [56, 66, 67]. Extracellular vesicles are membrane-bound, nanometer-sized particles released by every cell type and carrying bioactive signaling molecules from the parental cells [68]. Well established SASP factors are known to elicit both pro- and anti-tumorigenic immune responses, whereas senEVs are a very recent addition to the senescent cell secretome and may have been a confounding factor in previous SASP studies. Therefore, there is an urgent need to define the specific impact of senEVs on immune responses to senescence. Without such information, our ability to prevent cancer recurrence by targeting cellular senescence will likely remain limited.

The goal of the current study was to investigate the role of senEVs on senescence surveillance and to test the hypothesis that senEVs deliver important packets of information to immune cells. Our group pioneered the use of genetic tools to investigate the role of unmanipulated EVs within their *in vivo* microenvironment [53]. These approaches are changing how EVs are studied, enabling functional investigations in animal models. We have now adapted these strategies to dissect senEVs' influence on cancer recurrence from that of the SASP. To test if senEVs have a functional role in senescence surveillance and tumor formation/recurrence, we challenged mice with half million senEV-competent or senEV-deficient senescent cells (Figure 3). Our *in vitro* senescence induction protocol reduced total cell proliferation to 15% (as compared to untreated squamous carcinoma cells, Figure 1B), and slowed cell cycle down by a factor of 7 (after a 2-hour BrdU pulse, Figure 1B), which is equivalent to a 98% reduction in cell proliferation potential. To interfere with senEV release, we used a validated approach as discussed in the Results. Strikingly, senEV inhibition promoted tumor recurrence in two independent experiments, as compared to EV-competent senescent cells (Figure 3A). Of note, Rab35 manipulation did not influence senescence induction or exit from cell cycle (Figure 3B), suggesting no cell autonomous effects of senEV inhibition. To start investigating the fate of engrafted senescent cells in immune competent mice, we repeated the experiment and tracked the numbers of engrafted senescent cells using genetic markers 3 days after implantation (that is, when there is no visible tumor formation yet). We observed that senEV-competent senescent cells were quickly reduced to almost undetectable levels, whereas interfering with senEV release led to longer persistence of senescent cells, which was 5-fold higher than that of senEV-competent senescent cells, on average (Figure 3C). These results suggest that senEVs may play non-cell-autonomous roles in senescence immune surveillance by promoting senescent cell removal from tissues, which ultimately prevents cancer recurrence.

To functionally investigate the role of senEVs in senescence immune surveillance, we repeated the experiment above and challenged mice with half million senEV-competent or senEV-deficient senescent cells. After 3 days

(that is, when there is no tumor yet), we quantified the immune infiltrate, including CD4 and CD8 T cells and their type-1 effector subsets expressing T-bet, T regulatory cells, NK and NKT cells, myeloid cells including neutrophils, dendritic cells, macrophages and their subsets, and B cells. We observed a significant decrease (~50%) only in specific immune cell types, which were related only by the fact that they are all professional antigen presenting cells (APC); senEV inhibition decreased the fractions of infiltrating dendritic cells, B cells and MHC-II+ macrophages (Figure 3D). These results strongly indicate that senEVs are required to recruit APC to sites of senescence. Overall, these observations are consistent with a model in which senEVs promote immune surveillance of senescent cells. The recruitment of APC suggests that senEVs may represent a source of senescent cell antigens for adaptive responses. If senEV signaling is impaired, senescent cells will persist longer in tissues, which increases the chances of recurrence.

Using EV specific marker, Flotillin-1 and nanoparticle tracking analysis, we carefully validated that over-expression of Rab35-DN efficiently and specifically reduces EV release also in senescent cells (Figure 2A & B), while avoiding any unwanted impact on the SASP (Figure 2C). These results indicate that the profound inhibition of senEV release is suitable for functional studies. We optimized *in vitro* senescence induction in a way that enough senescent cells could be harvested for implantation in mice (Figure 1). To confirm generation of *bona fide* senescent cells, we assessed proliferation, apoptosis and cell death, or lack thereof in two distinct cell lines: MOC2 and mEER+. We treated the above squamous cell carcinoma lines with different dose combinations of cisplatin and/or paclitaxel and find out the optimal dose that induced senescence and decreased proliferation without induction of apoptosis or cell death (Figure 1 a& S1). Once implanted in mice, senescent cells would not be exposed to these chemotherapeutic drugs, we further validated that the senescent phenotype remained present for at least a week after removal of paclitaxel (Figure 1C), suggesting that *in vitro* generated senescent cells may remain senescent once in tissues. To test if, once *in vivo*, senescent cells would revert to squamous carcinoma cells and form a tumor, we compared tumor formation in immunocompetent syngeneic mice between untreated and paclitaxel-treated squamous senescent cells. We observed that paclitaxel treatment largely abated tumor formation, with small avascular masses only becoming visible after two weeks (Figure 1D), suggesting that we have a wide window of time (~10 days) to investigate senescent-immune cell interactions. Overall, these results validate our *in vivo* model system as a *bona fide* model of senescence.

Removal of senescent cells is mediated by immune responses [50]. The immune response found during senescence surveillance is believed to be different from that elicited within the tumor microenvironment [51, 52]. To test whether our engraftment-based model of senescence recapitulates these differences, we performed multiparameter flow cytometric analysis of oral tissues three days after they were engrafted with senescent or carcinoma cells. As control, we injected PBS. We observed significant differences in the immune infiltrates, as expected, T and NK cells were significantly increased within senescent oral tissues 3 days after challenge as compared to oral tissues seeded with tumorigenic cells (Figure 1E). We observed a significant shift in macrophage subsets, with an increase in the fraction of MHC-II– CD80+ CD206+ macrophages and a corresponding decrease in the MHC-II+ CD80– CD206– macrophages. Interestingly, B cells and dendritic cells were decrease in senescent tissues. All of the above-mentioned immune subsets were differentially recruited by tumor and senescent cells. On the contrary, neutrophils, regulatory (FoxP3+) and type-1 helper (Tbet+) T cells were coordinately recruited by both tumor and senescent cells (Figure 1E). These results suggest that our senescence model recapitulates expected immune responses and that there are shifts in immune cell infiltrates during senescence surveillance. These changes in immune composition may play important roles in the removal of senescent cells.

In order to identify which signals on senEVs may be responsible for recruiting and activating APC (Figure 3D), we compared EVs from senescent and tumor cells. We quantified protein content, numbers and size by mass-spectroscopy, electron microscopy and nanoparticle tracking analyses (Figure 4). Senescent cells released ~6-fold higher amounts of EVs per million cells, as measured by protein content, compared to non-senescent squamous carcinoma cells (Figure 4A). These results may be explained by either a higher rate of EV release by senescent cells, a bigger size, or higher amounts of proteins among their cargo, or a combination of the above. To discriminate between these alternatives, we performed nanoparticle tracking analysis (Figure 4B). After normalizing for cell numbers, we observed that senEVs had a 2-fold lower count compared to EVs from non-senescent cells (not shown), which resulted in a ~13-fold higher protein content per single EV (Figure 4B right). We observed a 16% increase in median diameter, as measured by nanoparticle tracking analysis (Figure 4B), which corresponds to a 60% increase in volume (assuming a spherical shape). Electron microscopy analysis confirmed that senEVs are 16% bigger than tumor EVs (Figure 4C). These results indicate that senEVs are bigger and pack more proteins, as compared to tumor EVs. The increase in senEV protein content and size suggests that they may carry important signals for immune cell recruitment and/or activation. To identify senEV-specific proteins that may signal to immune cells, we performed proteomic analyses. We scaled up senescent cell production *in vitro* (validation data not shown) and used mass spectroscopy to analyze EVs, in collaboration with the Pacific Northwest National Laboratories. We isolated EVs by ultracentrifugation from cell culture supernatants. In order to avoid contamination from fetal bovine serum EVs, we cultured the cells using EV-free serum. Proteomic analysis revealed 150 and 120 proteins differentially present in senEVs from MOC2 and mEER+ cells, respectively (as compared to EVs from non-senescent MOC2 and mEER+, Figure 4D). Proteins in senEVs were significantly associated with pathways involved in core cellular functions (Ribosomes, Spliceosome and DNA replication) but also with type-1 immunity (systemic lupus erythematosus; Figure 4E). Among the proteins found in common between mEER+ and MOC2 (which carry different mutations/oncogenes, see above), ribosomal proteins were the most common (Figure 4F). Overall, these results indicate that senEVs carry a unique set of molecules that may signal to immune cells.

Overall, the current study supports a scenario in which therapy-induced senescence promotes the release of senEVs, which contribute to senescence surveillance by recruiting antigen presenting cells. This pathway prevents cancer recurrence because in absence of senEVs senescent cells persist in tissues, which blocks recruitment of antigen presenting cells thereby promoting tumor relapse. Specific signals on senEVs may be responsible for antigen presenting cells' recruitment and/or activation.

Acknowledgements

NIH grant T32 CA254888 (TZ); Cancer Research UK C52489/A29681 (FP, NC);

References

1. Johnson, D.E., et al., *Head and neck squamous cell carcinoma.* Nat Rev Dis Primers, 2020. **6**(1): p. 92.
2. Siegel, R.L., K.D. Miller, and A. Jemal, *Cancer statistics, 2019.* CA Cancer J Clin, 2019. **69**(1): p. 7-34.
3. Torre, L.A., et al., *Global cancer statistics, 2012.* CA Cancer J Clin, 2015. **65**(2): p. 87-108.
4. Ferlay, J., et al., *Estimating the global cancer incidence and mortality in 2018: GLOBOCAN sources and methods.* Int J Cancer, 2019. **144**(8): p. 1941-1953.
5. Solomon, B., R.J. Young, and D. Rischin, *Head and neck squamous cell carcinoma: Genomics and emerging biomarkers for immunomodulatory cancer treatments.* Semin Cancer Biol, 2018. **52**(Pt 2): p. 228-240.

6. Pignon, J.P., et al., *Meta-analysis of chemotherapy in head and neck cancer (MACH-NC): an update on 93 randomised trials and 17,346 patients.* Radiother Oncol, 2009. **92**(1): p. 4-14.
7. Bernier, J., et al., *Postoperative irradiation with or without concomitant chemotherapy for locally advanced head and neck cancer.* N Engl J Med, 2004. **350**(19): p. 1945-52.
8. Cooper, J.S., et al., *Postoperative concurrent radiotherapy and chemotherapy for high-risk squamous-cell carcinoma of the head and neck.* N Engl J Med, 2004. **350**(19): p. 1937-44.
9. Ferris, R.L., et al., *Nivolumab for Recurrent Squamous-Cell Carcinoma of the Head and Neck.* N Engl J Med, 2016. **375**(19): p. 1856-1867.
10. Ewald, J.A., et al., *Therapy-induced senescence in cancer.* J Natl Cancer Inst, 2010. **102**(20): p. 1536-46.
11. Collado, M. and M. Serrano, *Senescence in tumours: evidence from mice and humans.* Nat Rev Cancer, 2010. **10**(1): p. 51-7.
12. Gewirtz, D.A., S.E. Holt, and L.W. Elmore, *Accelerated senescence: an emerging role in tumor cell response to chemotherapy and radiation.* Biochem Pharmacol, 2008. **76**(8): p. 947-57.
13. Wang, L., L. Lankhorst, and R. Bernards, *Exploiting senescence for the treatment of cancer.* Nat Rev Cancer, 2022. **22**(6): p. 340-355.
14. Demaria, M., et al., *Cellular Senescence Promotes Adverse Effects of Chemotherapy and Cancer Relapse.* Cancer Discov, 2017. **7**(2): p. 165-176.
15. Fletcher-Sananikone, E., et al., *Elimination of Radiation-Induced Senescence in the Brain Tumor Microenvironment Attenuates Glioblastoma Recurrence.* Cancer Res, 2021. **81**(23): p. 5935-5947.
16. Deschenes-Simard, X., et al., *Circumventing senescence is associated with stem cell properties and metformin sensitivity.* Aging Cell, 2019. **18**(2): p. e12889.
17. Duy, C., et al., *Chemotherapy Induces Senescence-Like Resilient Cells Capable of Initiating AML Recurrence.* Cancer Discov, 2021. **11**(6): p. 1542-1561.
18. Milanovic, M., et al., *Senescence-associated reprogramming promotes cancer stemness.* Nature, 2018. **553**(7686): p. 96-100.
19. Nacarelli, T., et al., *NAMPT Inhibition Suppresses Cancer Stem-like Cells Associated with Therapy-Induced Senescence in Ovarian Cancer.* Cancer Res, 2020. **80**(4): p. 890-900.
20. Calcinotto, A., et al., *Cellular Senescence: Aging, Cancer, and Injury.* Physiol Rev, 2019. **99**(2): p. 1047-1078.
21. Ruscetti, M., et al., *NK cell-mediated cytotoxicity contributes to tumor control by a cytostatic drug combination.* Science, 2018. **362**(6421): p. 1416-1422.
22. Li, F., et al., *FBP1 loss disrupts liver metabolism and promotes tumorigenesis through a hepatic stellate cell senescence secretome.* Nat Cell Biol, 2020. **22**(6): p. 728-739.
23. Rao, S.G. and J.G. Jackson, *SASP: Tumor Suppressor or Promoter? Yes!* Trends Cancer, 2016. **2**(11): p. 676-687.
24. Coussens, L.M. and Z. Werb, *Inflammation and cancer.* Nature, 2002. **420**(6917): p. 860-7.
25. Hanahan, D. and L.M. Coussens, *Accessories to the crime: functions of cells recruited to the tumor microenvironment.* Cancer Cell, 2012. **21**(3): p. 309-22.
26. Hanahan, D. and R.A. Weinberg, *Hallmarks of cancer: the next generation.* Cell, 2011. **144**(5): p. 646-74.
27. Guillon, J., et al., *Chemotherapy-induced senescence, an adaptive mechanism driving resistance and tumor heterogeneity.* Cell Cycle, 2019. **18**(19): p. 2385-2397.
28. Krtolica, A., et al., *Senescent fibroblasts promote epithelial cell growth and tumorigenesis: a link between cancer and aging.* Proc Natl Acad Sci U S A, 2001. **98**(21): p. 12072-7.
29. Borghesan, M., et al., *Small Extracellular Vesicles Are Key Regulators of Non-cell Autonomous Intercellular Communication in Senescence via the Interferon Protein IFITM3.* Cell Rep, 2019. **27**(13): p. 3956-3971 e6.
30. Kadota, T., et al., *Emerging role of extracellular vesicles as a senescence-associated secretory phenotype: Insights into the pathophysiology of lung diseases.* Mol Aspects Med, 2018. **60**: p. 92-103.

31. Misawa, T., et al., *Biology of extracellular vesicles secreted from senescent cells as senescence-associated secretory phenotype factors.* Geriatr Gerontol Int, 2020. **20**(6): p. 539-546.
32. Terlecki-Zaniewicz, L., et al., *Small extracellular vesicles and their miRNA cargo are anti-apoptotic members of the senescence-associated secretory phenotype.* Aging (Albany NY), 2018. **10**(5): p. 1103-1132.
33. Veziroglu, E.M. and G.I. Mias, *Characterizing Extracellular Vesicles and Their Diverse RNA Contents.* Front Genet, 2020. **11**: p. 700.
34. Onken, M.D., et al., *A surprising cross-species conservation in the genomic landscape of mouse and human oral cancer identifies a transcriptional signature predicting metastatic disease.* Clin Cancer Res, 2014. **20**(11): p. 2873-84.
35. Vermeer, D.W., et al., *Metastatic model of HPV+ oropharyngeal squamous cell carcinoma demonstrates heterogeneity in tumor metastasis.* Oncotarget, 2016. **7**(17): p. 24194-207.
36. Debacq-Chainiaux, F., et al., *Protocols to detect senescence-associated beta-galactosidase (SA-betagal) activity, a biomarker of senescent cells in culture and in vivo.* Nat Protoc, 2009. **4**(12): p. 1798-806.
37. Rothaeusler, K. and N. Baumgarth, *Evaluation of intranuclear BrdU detection procedures for use in multicolor flow cytometry.* Cytometry A, 2006. **69**(4): p. 249-59.
38. Kornilov, R., et al., *Efficient ultrafiltration-based protocol to deplete extracellular vesicles from fetal bovine serum.* J Extracell Vesicles, 2018. **7**(1): p. 1422674.
39. Nakayasu, E.S., et al., *MPLEx: a Robust and Universal Protocol for Single-Sample Integrative Proteomic, Metabolomic, and Lipidomic Analyses.* mSystems, 2016. **1**(3).
40. Matos Baltazar, L., et al., *Antibody Binding Alters the Characteristics and Contents of Extracellular Vesicles Released by Histoplasma capsulatum.* mSphere, 2016. **1**(2).
41. Cox, J. and M. Mann, *MaxQuant enables high peptide identification rates, individualized p.p.b.-range mass accuracies and proteome-wide protein quantification.* Nat Biotechnol, 2008. **26**(12): p. 1367-72.
42. Schwanhausser, B., et al., *Global quantification of mammalian gene expression control.* Nature, 2011. **473**(7347): p. 337-42.
43. Shetty, A.V. and D.J. Wong, *Systemic Treatment for Squamous Cell Carcinoma of the Head and Neck.* Otolaryngol Clin North Am, 2017. **50**(4): p. 775-782.
44. Stransky, N., et al., *The mutational landscape of head and neck squamous cell carcinoma.* Science, 2011. **333**(6046): p. 1157-60.
45. Anderson, G., et al., *An Updated Review on Head and Neck Cancer Treatment with Radiation Therapy.* Cancers (Basel), 2021. **13**(19).
46. de Souza Viana, L., et al., *Efficacy and safety of a cisplatin and paclitaxel induction regimen followed by chemoradiotherapy for patients with locally advanced head and neck squamous cell carcinoma.* Head Neck, 2016. **38 Suppl 1**: p. E970-80.
47. Itahana, K., J. Campisi, and G.P. Dimri, *Methods to detect biomarkers of cellular senescence: the senescence-associated beta-galactosidase assay.* Methods Mol Biol, 2007. **371**: p. 21-31.
48. Gonzalez-Gualda, E., et al., *A guide to assessing cellular senescence in vitro and in vivo.* FEBS J, 2021. **288**(1): p. 56-80.
49. Ogrodnik, M., *Cellular aging beyond cellular senescence: Markers of senescence prior to cell cycle arrest in vitro and in vivo.* Aging Cell, 2021. **20**(4): p. e13338.
50. Kale, A., et al., *Role of immune cells in the removal of deleterious senescent cells*, in *Immunity and Ageing*. 2020, BioMed Central Ltd.
51. Gieseck, R.L., M.S. Wilson, and T.A. Wynn, *Type 2 immunity in tissue repair and fibrosis*, in *Nature Reviews Immunology*. 2018, Nature Publishing Group. p. 62-76.
52. Shiao, S.L., et al., *TH2-Polarized CD4(+) T Cells and Macrophages Limit Efficacy of Radiotherapy.* Cancer Immunol Res, 2015. **3**(5): p. 518-25.

53. Pucci, F., et al., *SCS macrophages suppress melanoma by restricting tumor-derived vesicle-B cell interactions.* Science, 2016. **352**(6282): p. 242-6.
54. Hsu, C., et al., *Regulation of exosome secretion by Rab35 and its GTPase-activating proteins TBC1D10A–C*, in *J Cell Biol*. 2010. p. 223-32.
55. Yang, L., et al., *Long non-coding RNA HOTAIR promotes exosome secretion by regulating RAB35 and SNAP23 in hepatocellular carcinoma*, in *Mol Cancer*. 2019.
56. Coppe, J.P., et al., *The senescence-associated secretory phenotype: the dark side of tumor suppression.* Annu Rev Pathol, 2010. **5**: p. 99-118.
57. Guccini, I., et al., *Senescence Reprogramming by TIMP1 Deficiency Promotes Prostate Cancer Metastasis.* Cancer Cell, 2021. **39**(1): p. 68-82 e9.
58. Eggert, T., et al., *Distinct Functions of Senescence-Associated Immune Responses in Liver Tumor Surveillance and Tumor Progression.* Cancer Cell, 2016. **30**(4): p. 533-547.
59. Georgilis, A., et al., *PTBP1-Mediated Alternative Splicing Regulates the Inflammatory Secretome and the Pro-tumorigenic Effects of Senescent Cells.* Cancer Cell, 2018. **34**(1): p. 85-102 e9.
60. Ruscetti, M., et al., *Senescence-Induced Vascular Remodeling Creates Therapeutic Vulnerabilities in Pancreas Cancer.* Cell, 2020. **181**(2): p. 424-441 e21.
61. Lehmann, B.D., et al., *Senescence-associated exosome release from human prostate cancer cells.* Cancer Res, 2008. **68**(19): p. 7864-71.
62. Contrepois, K., et al., *Histone variant H2A.J accumulates in senescent cells and promotes inflammatory gene expression.* Nat Commun, 2017. **8**: p. 14995.
63. Kim, K.M., et al., *Identification of senescent cell surface targetable protein DPP4.* Genes Dev, 2017. **31**(15): p. 1529-1534.
64. Campisi, J., *Senescent cells, tumor suppression, and organismal aging: good citizens, bad neighbors.* Cell, 2005. **120**(4): p. 513-22.
65. Chakradeo, S., L.W. Elmore, and D.A. Gewirtz, *Is Senescence Reversible?* Curr Drug Targets, 2016. **17**(4): p. 460-6.
66. Hernandez-Segura, A., J. Nehme, and M. Demaria, *Hallmarks of Cellular Senescence*, in *Trends in Cell Biology*. 2018, Elsevier Ltd. p. 436-453.
67. Salama, R., et al., *Cellular senescence and its effector programs.* Genes Dev, 2014. **28**(2): p. 99-114.
68. Mathieu, M., et al., *Specificities of secretion and uptake of exosomes and other extracellular vesicles for cell-to-cell communication.* Nat Cell Biol, 2019. **21**(1): p. 9-17.

Figure 1. Validation of *in vitro* senescence induction with chemotherapeutic agents. A) MOC2 squamous carcinoma cells were treated with the indicated concentration of paclitaxel and cisplatin for 2 days (n=4). **B)** Cell proliferation during culture with 600 nM of paclitaxel (n=4) **C)** Persistence of senescence after removal of paclitaxel *in vitro* (mEER+) **D)** Implantation of untreated MOC2 (tumor cells) or paclitaxel-treated senescent MOC2 (senescent cells) in the dermis of mice (n=10). **E)** Immune subsets infiltrating tumor cells (TC) or senescent cells (SC) 3 days after implantation in the tongue. MOC2 +/- paclitaxel 600 nM. N=10. Statistics by two-way ANOVA with multiple testing correction.

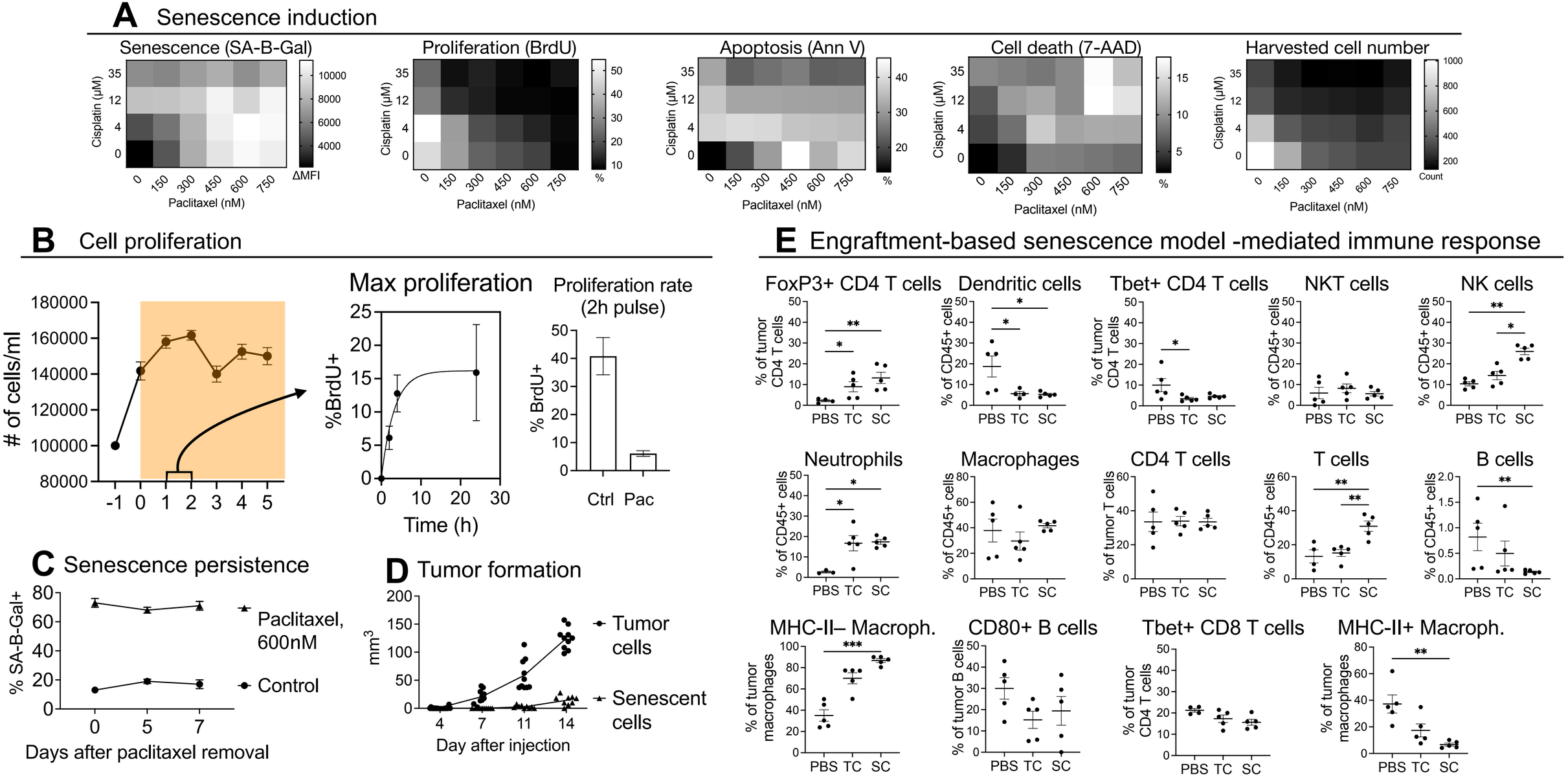

Figure 2. Validation of EV inhibition in senescent cells A) Immunoblot for EV marker Flotillin-1 on EV isolated by ultracentrifugation fro supernatant of cell lines carrying the indicated Rab35 (UT): untransduced). **B)** Nanoparticle tracking analysis by light scatter (top) and fluorescence (bottom) of EV samples as in A. **C)** Protein array-based semi-quantitative measurement of soluble mediators from senescent cells carrying the indicated Rab35 (n+2 independent experiments), Statistical test by two-way ANOVA.

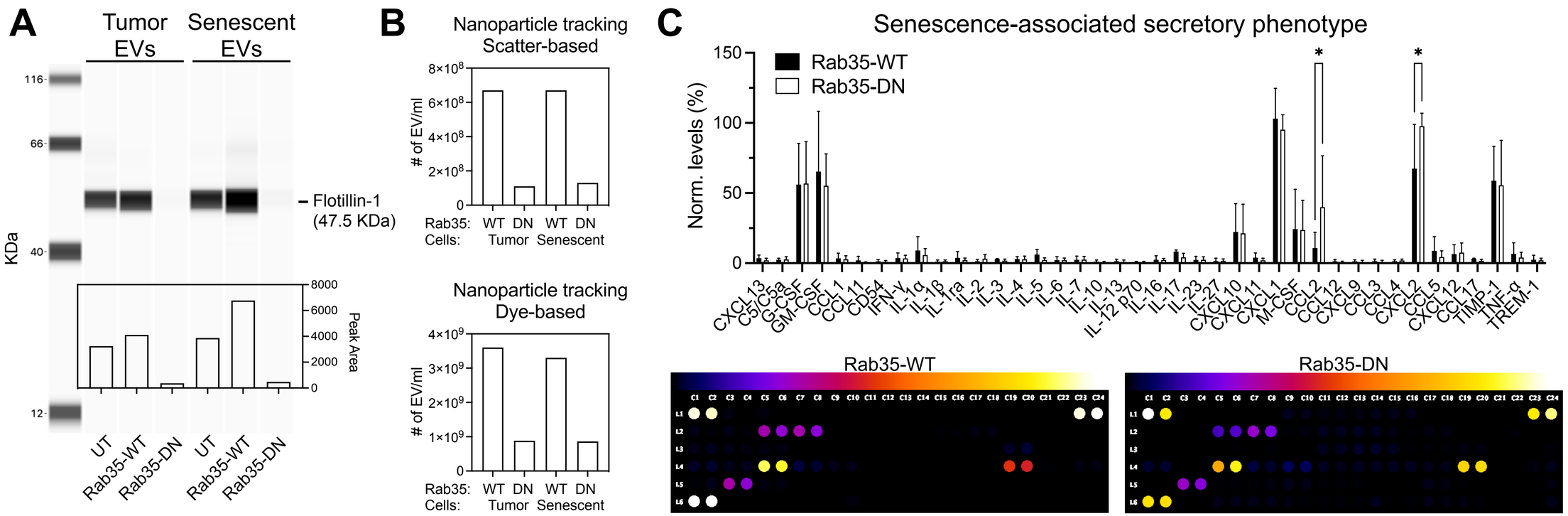

Figure 3. Senescent cell-derived EVs inhibit cancer recurrence by recruiting three different antigen presenting cell subsets. **A)** senEV inhibition (Rab 35-DN) promotes orthotropic and flank tumor formation. **B)** interfering with senEV release does not affect senescence induction (top) or proliferation arrest (bottom) in vitro. **C)** interfering with senEV release promotes persistence of senescent cells in oral tissues **D)** senEVs are required to recruit professional antigen presenting cells to sites of oral senescence. Statistical testes by one-way ANOVA or Mann-Whitney.

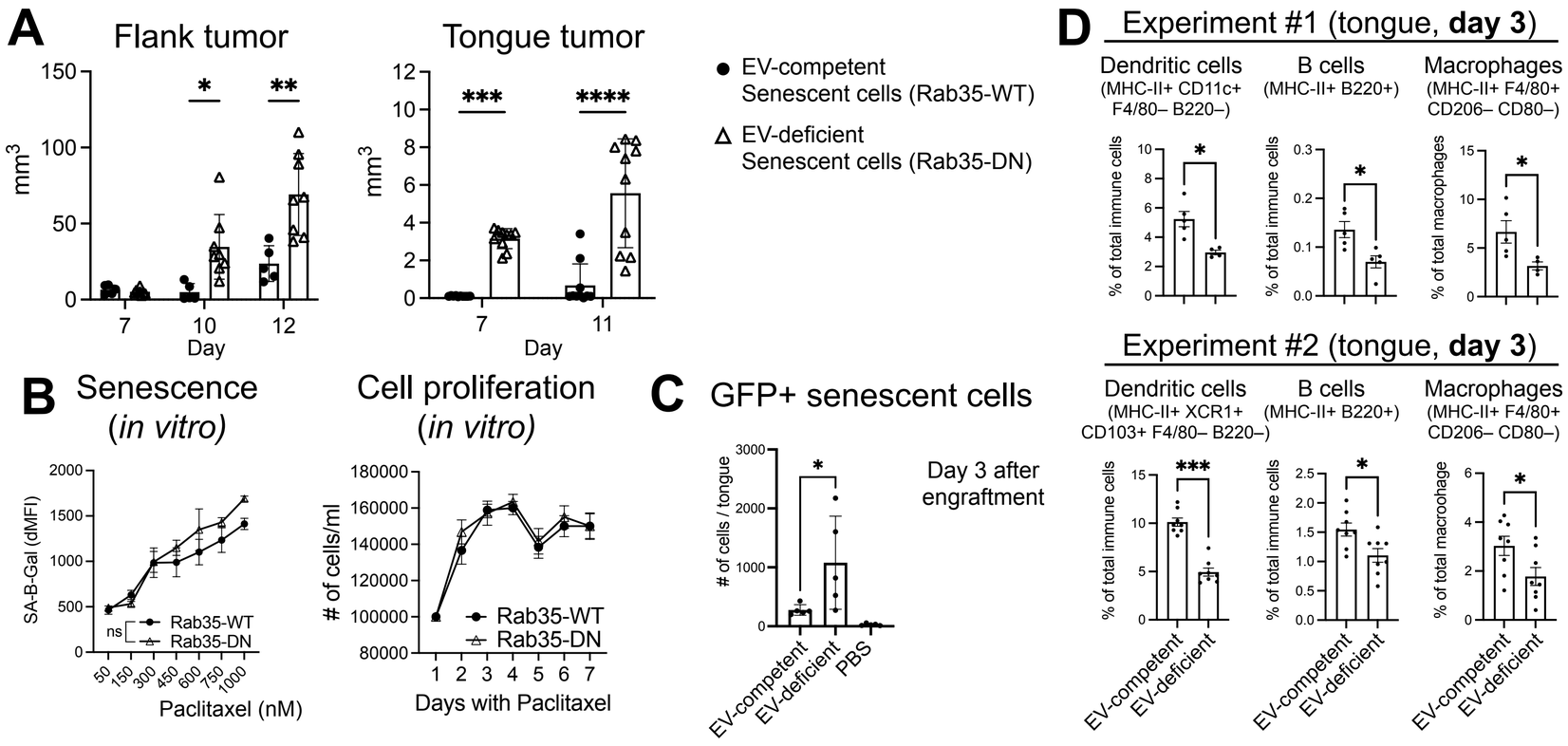

Figure 4. Characterization of senEVs and identification of candidate ligands for immune cell engagement. A) Protein content normalized for cell number (mEER+). **B)** Size and count of senEVs by nanoparticle tracking analysis (Zetaview) **C)** Size by electron microscopy **D)** Differential presence of proteins on sen EVs (as compared to EVs from non-senescent cells) **E)** Gene ontology analysis of enriched pathways on senEVs (n=3; mEER+) **F)** Common proteins found enriched (or depleted) in senEVs from MOC2 and mEER+. Statistical tests by Mann-Whitney or one-way ANOVA. Proteomic analysis multiple comparisons corrected by Benjamin, Krieger and Yekkutieli.

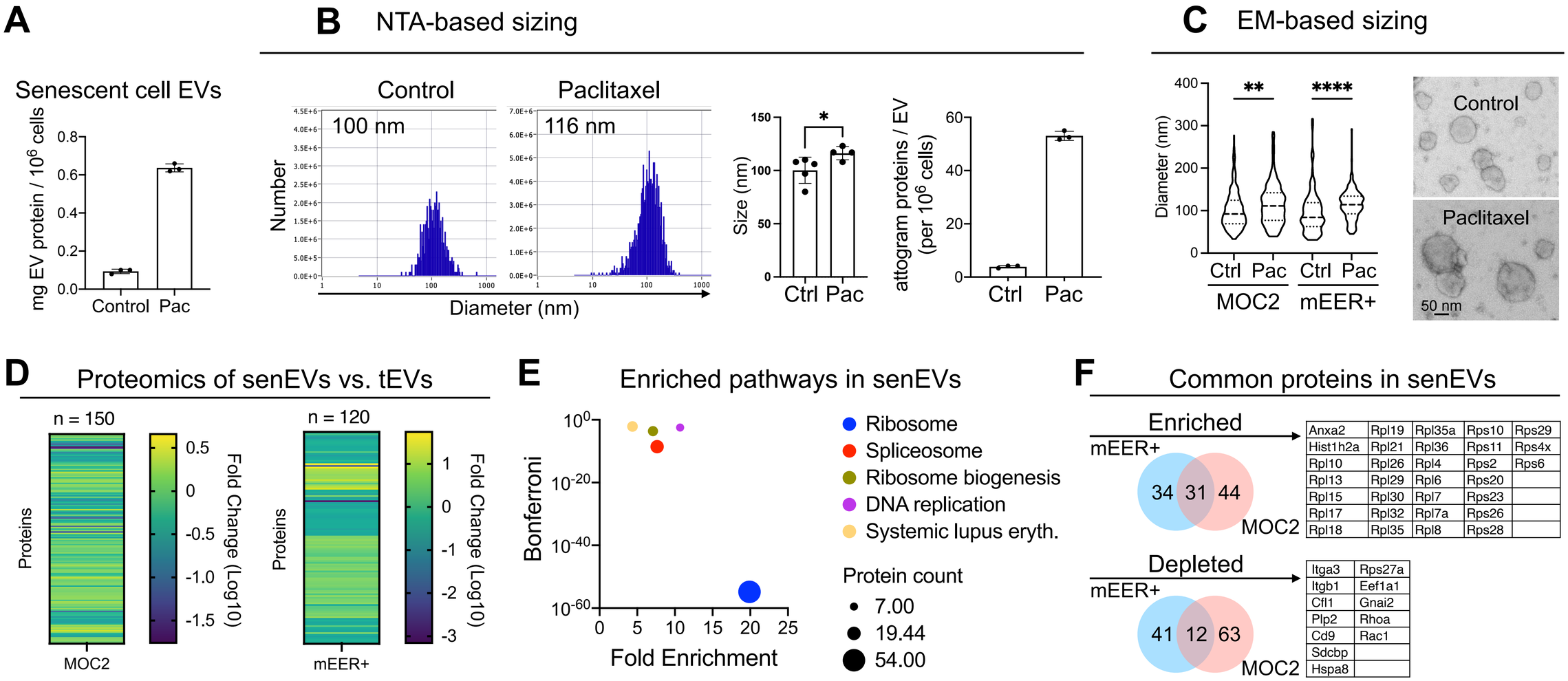

Figure S1. Validation of *in vitro* senescence induction with chemotherapeutic agents. A) mEER+ squamous carcinoma cells were treated with the indicated concentration of paclitaxel and cisplatin for 2 days (n=4).

A Senescence induction

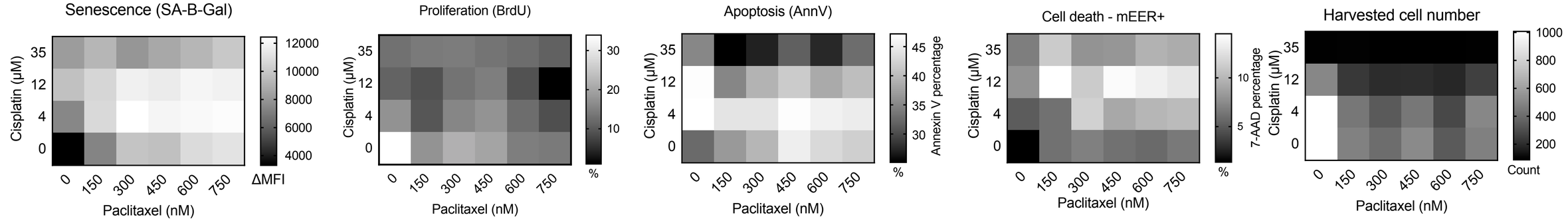

B Examples of images of control and senescent cells

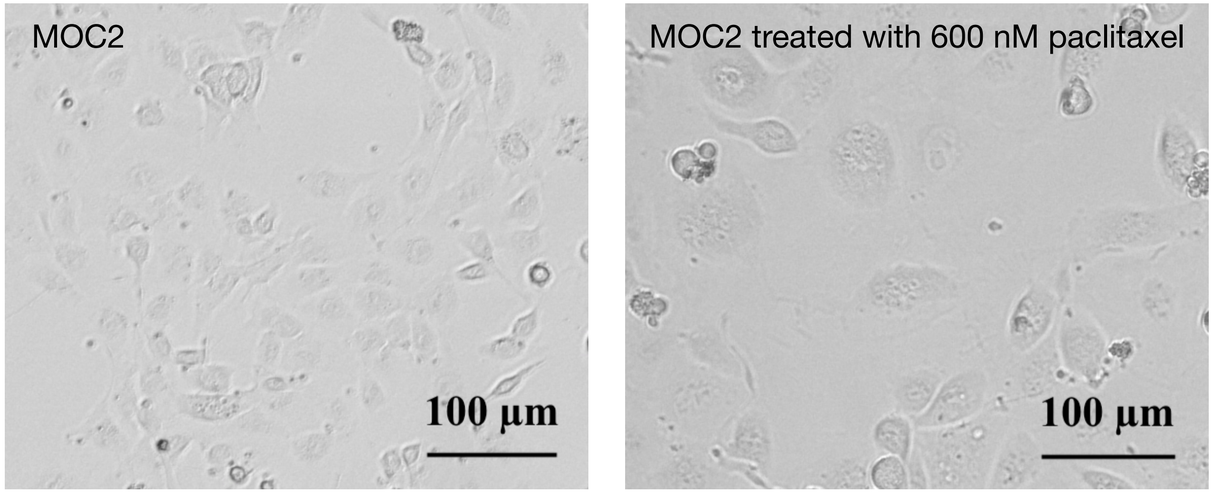
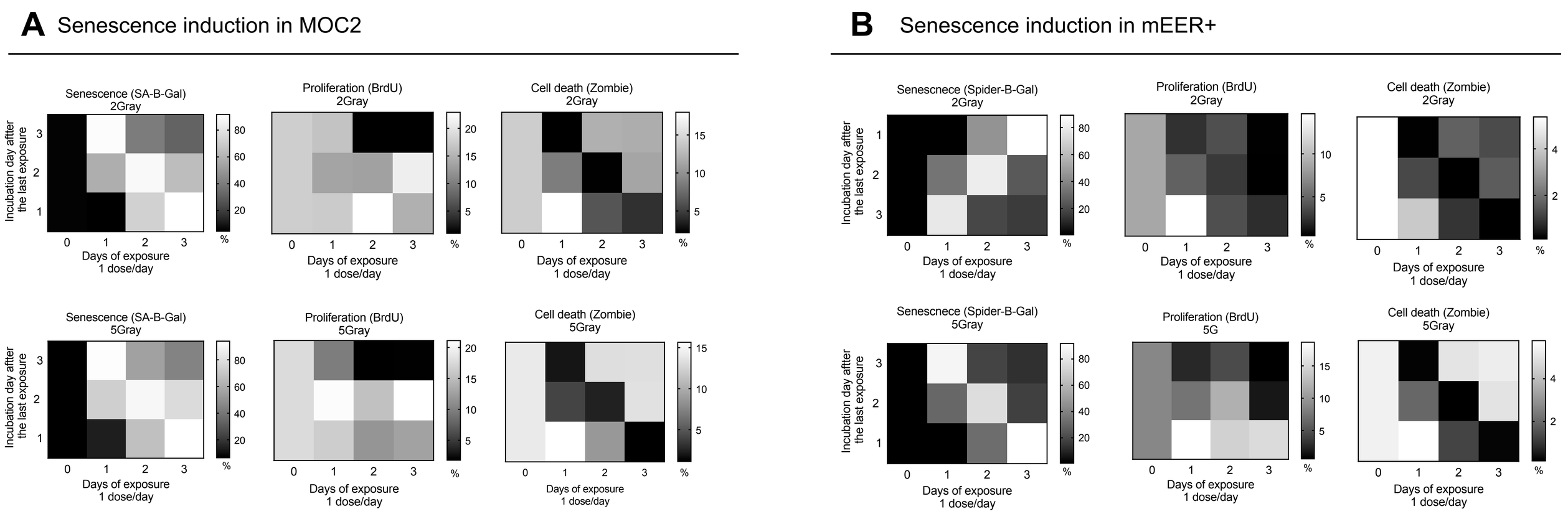
Figure S2. *In vitro* senescence induction with X-ray irradiation (2 and 5 Gray). MOC2 squamous carcinoma cells were treated with 1, 2, or 3, doses of 2 or 5 Gray and incubated for 1, 2, or 3 days after the last exposure (n=4).